A Novel Retrieval Algorithm for Cloud Optical Properties from the Atmospheric Radiation Measurement Two-Channel Narrow-Field-of-View Radiometer

W.J. Wiscombe, and A. Marshak
NASA Goddard Space Flight Center
Greenbelt, Maryland

J.C. Chiu
Joint Center for Earth Systems Technology/UMBC
Need location

Y. Knyazikhin
Boston University
Boston, Massachusetts

J. Barnard
Pacific Northwest National Laboratory
Richland, Washington

Y. Luo
Noetix Research Inc.
Ottawa, Ontario
Canada

Introduction

Cloud optical depth is one of the most important cloud optical properties, and is vital for any cloud-radiation parameterization. To estimate cloud optical depth, the atmospheric science community in the past decade has widely used ground-based flux measurements from either broadband (Leontieva and Stamnes 1994, Boers 1997) or narrowband (Min and Harrison 1996, Leontieva and Stamnes 1996) radiometers. However, this type of technique is limited to overcast conditions, and at best, gives an "effective" cloud optical depth instead of its "local" value (Ricchiazzi et al. 1995, Dong et al. 1997).

Unlike flux instruments, narrow field-of-view (NFOV) radiometers that measure zenith radiance have the potential to provide less effective, more local cloud optical properties. However, it is known that even in 1D plane-parallel theory the relationship between cloud optical depth and zenith radiance is a double-valued function (as shown in Figure 1). This indicates that it is impossible in general to unambiguously retrieve cloud optical depth from just a one-channel NFOV radiometer.

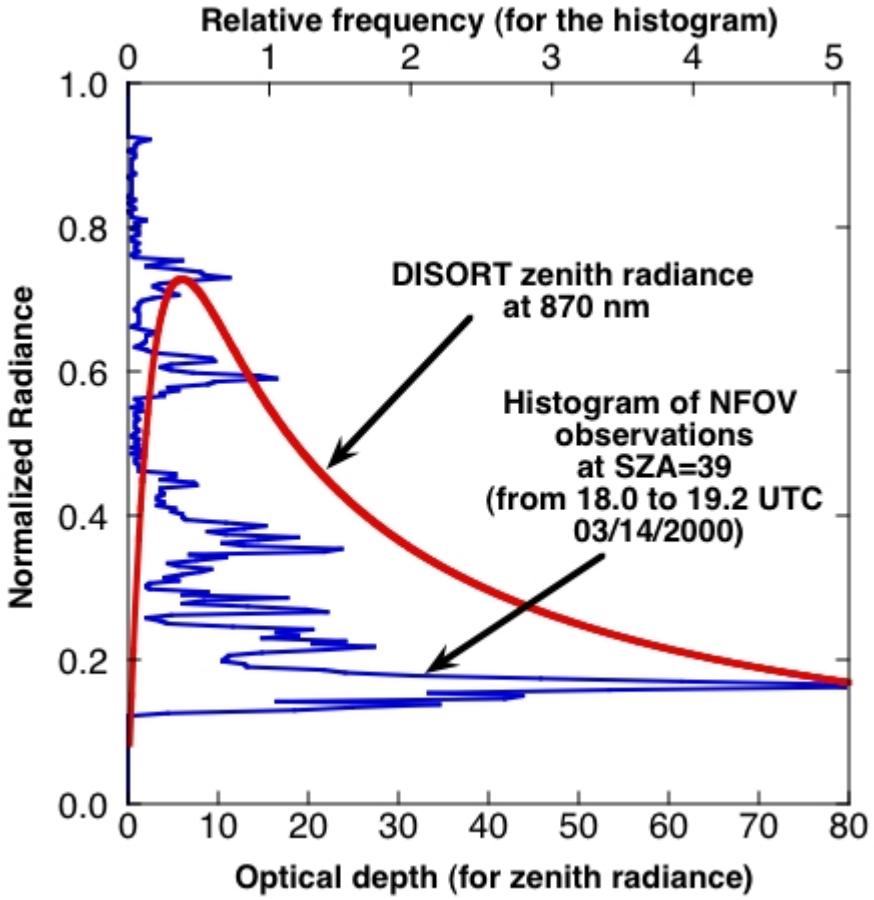

Figure 1. Downward 870 nm radiances vs. cloud optical depth (lower x-axis) calculated by DISORT with a surface albedo of 0.271. Co-Plotted blue curve is a histogram of the ARM one-channel NFOV radiances (870 nm) from 18 to 19.2 UTC, March 14, 2000, using the upper x-axis.

Figure 1 shows another problem with inferring optical depth from monochromatic zenith radiance. The histogram of actual observations from the one-channel NFOV radiometer of the Atmospheric Radiation Measurement (ARM) program reveals that some values of NFOV radiances are higher than any possible 1D radiance due to 3D effects. This strong influence of cloud inhomogeneous structures on zenith radiance also seen in simulations of a 3D Monte Carlo radiative transfer model (referred to Figure 2 in Marshak et al. 2004) makes some radiances not retrievable.

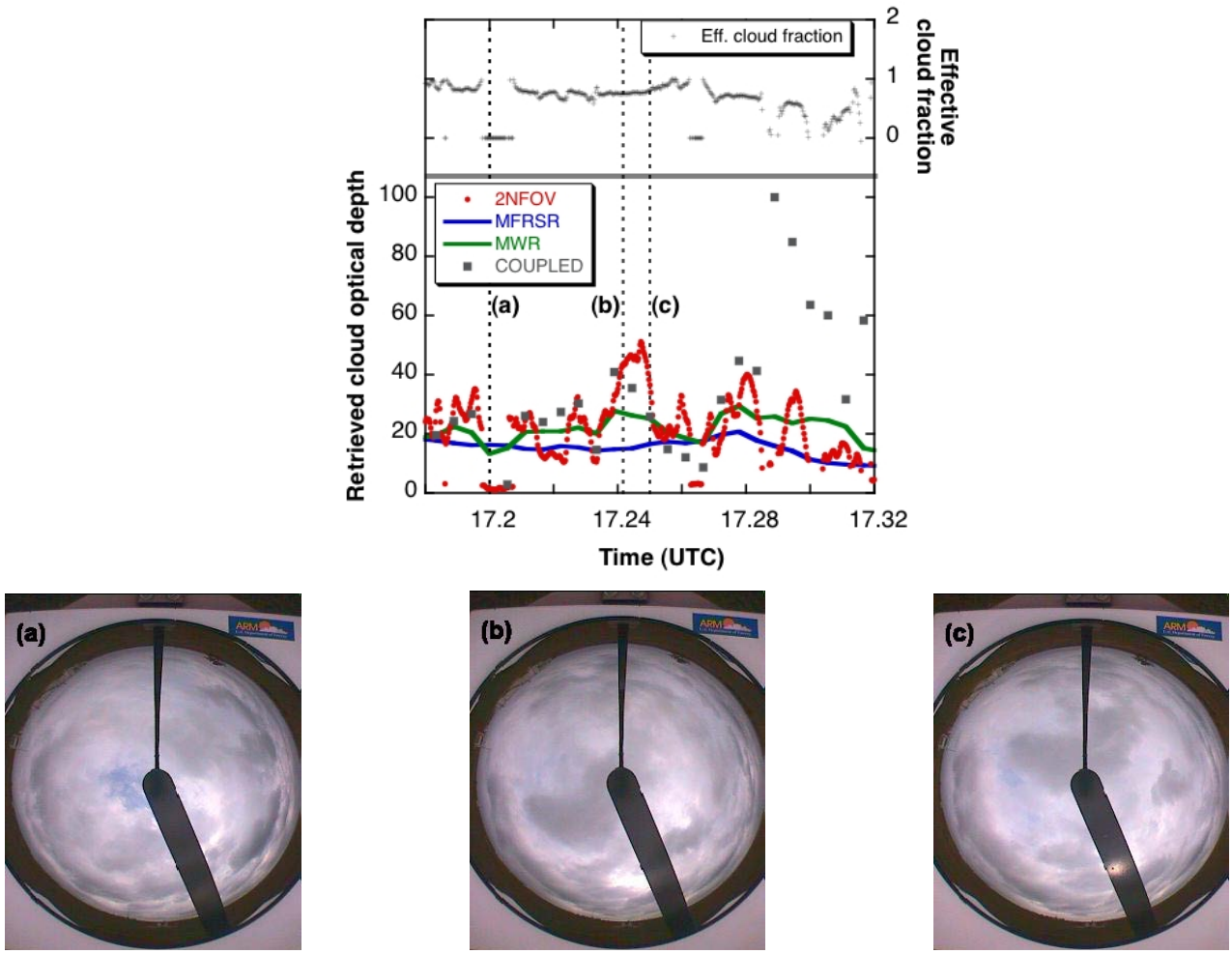

Figure 2. Retrieved cloud optical depths (left y-axis) and effective cloud fractions (right y-axis) at the SGP site for October 28, 2004, estimating from the 2NFOV, MFRSR, MWR, and the COUPLED algorithm. Retrieved effective cloud fractions are added at the top panel. Dash lines indicate the time when TSI snapshots were taken: (a) 17:12:00, (b) 17:14:30, and (c) 17:15:00 UTC.

To reduce the retrieval ambiguity of radiance-based algorithms, Marshak et al. (2004) proposed estimating cloud optical depths from two channel radiance (673 nm [RED] and 870 nm [NIR]) measurements. The underlying principle of their algorithm is that these two channels have similar cloud properties but strong spectral contrast in surface reflectance. They look up observations directly on a plane of RED vs. NIR radiances calculated from a plane-parallel model. Their approach leads to the retrieval of not only cloud optical depths, but also "effective" cloud fractions. We refer hereafter to this algorithm as the "RED vs. NIR" algorithm.

To solve the lack of a one-to-one relationship in radiance-based algorithms, Barker and Marshak (2001) proposed a different approach. They coupled radiances along with flux measurements. In this paper we call it the "COUPLED" algorithm. Their method has been tested in model-generated clouds and associated radiation fields. To assess the performance of this algorithm in more realistic conditions,

Barker et al. (2004) have evaluated cloud optical depth retrievals with cloud model-generated data that release the frozen turbulence assumption used in Barker and Marshak (2001).

The ARM program deployed a new two-channel Narrow Field-of-View Radiometer (2NFOV) at the Southern Great Plains (SGP) central facility in September 2004. This radiometer is a ground-based instrument that measures downwelling zenith radiance at 673 and 870 nm. It has a 5.7° field of view and a one-second temporal resolution. From measurements of the 2NFOV radiometer, we can advance our understanding of the performance of the aforementioned algorithms in real-world applications. Most importantly, we have the first chance to capture local rapid changes of 3D cloud structures at the natural time scale of clouds.

The objective of this paper is to illustrate cloud evolution with high temporal resolution retrievals that are yielded mainly from the "RED vs. NIR" algorithm. To put the performance of this algorithm into context, we compare our retrievals with those estimated from the ARM Multi-Filter Rotating Shadowband Radiometer (MFRSR), the microwave radiometer (MWR), and the COUPLED algorithm that uses both radiances and fluxes.

Algorithm descriptions

a. RED vs. NIR algorithm

Any ground-based measurements of radiance I can be given as (pp. 365-366, Liou 2002)

$$I = I_o + \frac{\rho T_o I_s}{1 - \rho R}, \tag{1}$$

where the first term I_0 on the right side represents the radiation calculated for a non-reflecting surface, and the second term is the radiation due to interactions between clouds and the surface. The surface-cloud interactions depend on the albedo ρ of the underlying Lambertian surface, the transmittance T_0 for a nonreflecting surface, the radiation I_s from an isotropic source located at the surface, and the spherical albedo of clouds R when illuminated from below upwelling isotropic radiation. By approximating the transmittance T_0 with

$$T_o = 1 - A_c + T_{o,pp} \cdot A_c \tag{2}$$

where A_c is the cloud fraction and $T_{0,pp}$ is the transmittance for non-reflecting surface in a plane-parallel assumption, we can rewrite Equation (1) as

$$I(\tau, A_c) = I_o(\tau) + \frac{\rho I_s(\tau)\left[1 - A_c + A_c T_{o,pp}(\tau)\right]}{1 - \rho R(\tau)}. \tag{3}$$

Note that the Ac is not a real cloud fraction, but rather a "radiatively effective" value that forces measurements taken from a 3D space fit into 1D plane-parallel radiative transfer calculations. Note that

we assume here that the dependency of zenith radiance on Ac comes only from Equation (2). Detailed discussions can be found in Marshak et al. (2004).

As expected from Equation (1), surface albedo has a strong impact on determining the radiances of our lookup tables, and thus on our retrievals. In this paper, we used surface albedo products generated by the Canada Centre for Remote Sensing Center (Luo et al. 2005). We further used the discrete ordinates radiative transfer (DISORT) to calculate $I(\tau, A_c)$ (Equation [3]) over a reasonable range of optical depths and effective cloud fractions. By comparing radiance measurements with 2D lookup tables, we infer both cloud optical depth and effective cloud fraction simultaneously.

b. The COUPLED algorithm

For plane-parallel clouds over a horizontally homogeneous Lambertian surface with a surface albedo ρ, transmittance T can be written as (Petty 2004, pp. 413)

$$T = \frac{T_o}{1 - \rho R}. \tag{4}$$

Combining Equations (1) and (4), we obtain

$$\begin{aligned} I_1 &= I_{o,1} + \rho_1 T_1 I_{s,1}, \\ I_2 &= I_{o,2} + \rho_2 T_2 I_{s,2}, \end{aligned} \tag{5}$$

where subscripts 1 and 2 represent wavelengths λ1 and λ2, respectively. If two wavelengths with similar cloud properties are selected, thus

$$\begin{aligned} I_{o,1} &\approx I_{o,2} \\ I_{s,1} &\approx I_{s,2} \approx I_s. \end{aligned} \tag{6}$$

It yields

$$I_2 - I_1 = (\rho_2 T_2 - \rho_1 T_1) I_s(\tau). \tag{7}$$

For a horizontally Lambertian surface the transmittance T related to the upwelling flux by

$$F_{up} = \rho T F_o, \tag{8}$$

where F_0 is the solar constant at a given wavelength. Define $F^{\uparrow}$ as the upward flux normalized by F_0. For simplicity, we also normalized I_1, I_2, and I_s, then Equation (7) can be rewritten as

$$I_2 - I_1 = (F_2^{\uparrow} - F_1^{\uparrow}) I_s(\tau), \tag{9}$$

Or

$$I_s(\tau);\ \frac{I_2 - I_1}{F_2^{\uparrow} - F_1^{\uparrow}}. \tag{10}$$

For general inhomogeneous clouds, we can derive a similar equation. Details are given in Knyazikhin et al. (2005).

Since MFRSR provides downwelling fluxes only, Equation (10) cannot be applied directly for cloud optical depth retrieval. The upwelling fluxes can be obtained from integrating all radiances that are reflected by the surface and reach to the cloud base. Barker and Marshak (2001) used a weighting function to approximate the integration. Once $F^{\uparrow}$ was ready, we derived I_s based on Equation (10). This observed normalized I_s was then compared with lookup tables to infer the cloud optical depth.

Results

The performance of the RED vs. NIR and the COUPLED algorithms in various cloud situations is described in this section, along with two other benchmark algorithms. The first benchmark algorithm is based on ARM MFRSR measurements (Min and Harrison 1996). The MFRSR provides spectral measurements of total solar flux at 415, 500, 615, 673, 870, and 940 nm every 20 seconds. We infer cloud optical depths from observed atmospheric transmittances derived from downward fluxes.

The second benchmark algorithm estimates cloud optical depth from microwave-retrieved liquid water path. The ARM microwave radiometer (MWR) measures brightness temperatures at 23.8 and 31.4 GHz every 20 seconds, and it has a 5.9° of FOV that is comparable to the 2NFOV radiometer (5.7°). Since an 8 μm effective radius of clouds (typical for the ARM Oklahoma ARM site) was assumed to construct lookup tables for the RED vs. NIR, and the COUPLED algorithms, we applied the same effective radius in the conversion of liquid water path to cloud optical depth.

Three of these algorithms retrieve cloud optical depths only; the RED vs. NIR algorithm additionally gives an effective cloud fraction. For illustration, we add sky images that were taken every 30 seconds by the ARM Total Sky Imager (TSI). This section will demonstrate the ability of the RED vs. NIR algorithm to capture cloud optical properties in great detail for fully 3D cloud situations.

a. Overcast

Figure 2 depicts an overcast case in which clouds show considerable inhomogeneity. A corresponding distribution of radiance measurements on our 2D lookup table is also plotted in Figure 3, showing that most observations fall into our lookup table. Data points with a larger radiance at 670 nm than 870 nm correspond to clear-sky situations.

In general, there is a great similarity among all retrievals. In particular, the RED vs. NIR algorithm captures detailed cloud evolutions and advections. For example, the TSI image shows a clear-sky hole around the 2NFOV location at 17:12:00 UTC (Figure 2a). This hole corresponds to a small retrieved

cloud optical depth and a zero effective cloud fraction. Two and half minutes later, a darker cloud in the left-bottom quadrant of the center is present and passes toward the right-upper quadrant (Figure 2b, c).

This much darker cloud, compared to its surrounding clouds, has resulted in a peak in the time series of retrieved cloud optical depths. This peak also appears in retrievals from the COUPLED algorithm. The microwave radiometer seems to detect this dark cloud, but with a much smaller sensitivity.

In the later period, retrievals from the COUPLED algorithm show significant fluctuations compared to others, and hence this algorithm deserves more discussions here. First, the performance of this algorithm relies on the absolute accuracy of both radiance and flux measurements. Any uncertainty in radiance and flux at these two channels are not necessarily cancelled out during the retrieval process (as shown in Equation [10]). Second, this algorithm uses time series of downward flux measurements to model the spatial distribution of the upwelling fluxes for the point of interest. Therefore, assumptions in this approximation, including specifications of the time window, cloud advection speed and direction, and the model itself, might lead to misrepresentation of cloud situations. In short, retrievals from the COUPLED algorithm are determined by current local cloud property, as well as the previous and later measurements. As we can see in retrievals, for example, at 17.29 UTC, the unrealistic large cloud optical depth (up to 100) is apparently arisen from the large cloud optical depths at 17.28 and 17.295 UTC.

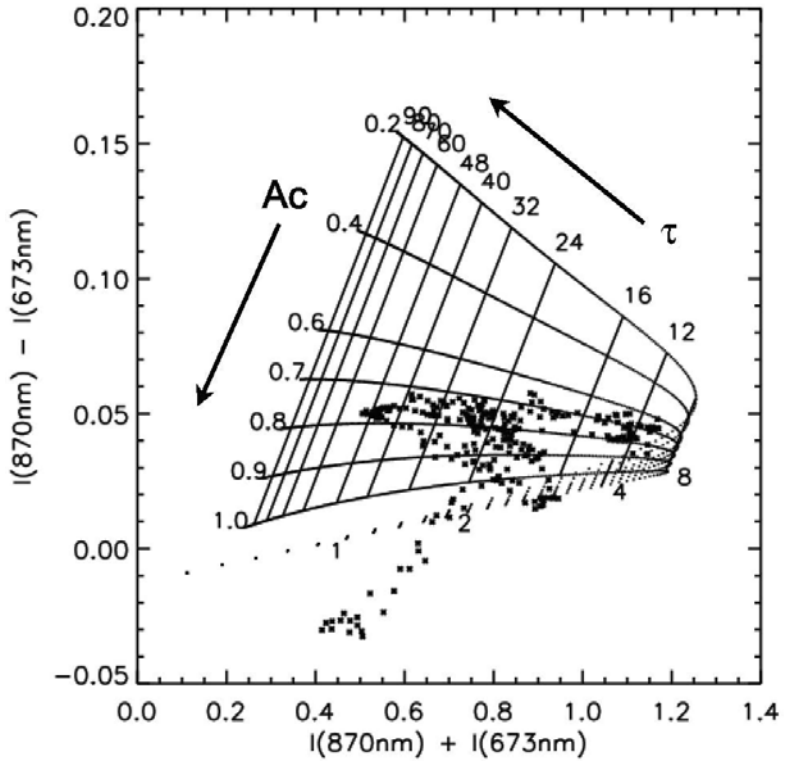

Figure 3. A lookup table (lines) constructed with a given solar zenith angle of 52°; effective radius of 8 μm; surface albedo of 0.13 and 0.28 for RED and NIR channels, respectively. The ARM 2NFOV measurements at the SGP site for 17:12:00-17:17:00 UTC, 2004/10/28 are also plotted by dots.

b. Broken clouds

Figure 4 demonstrates retrievals of a patchy cloud for 21:36 to 21:42 UTC, September 29, 2004. Some small cumulus clouds surrounded the outer ring of the center of the TSI images for most of the period. During 21:37 to 21:39, a patchy cloud passed by and was detected by the RED vs. NIR algorithm with an optical depth of around 3. Other algorithms are not sensitive enough to detect this cloud. Note that since at a small optical depth, contours with various effective cloud fractions are very close to each other in our lookup tables (as shown in Figure 3), an effective cloud fraction cannot be retrieved accurately here. Therefore, the values of effective cloud fractions are not shown for this case.

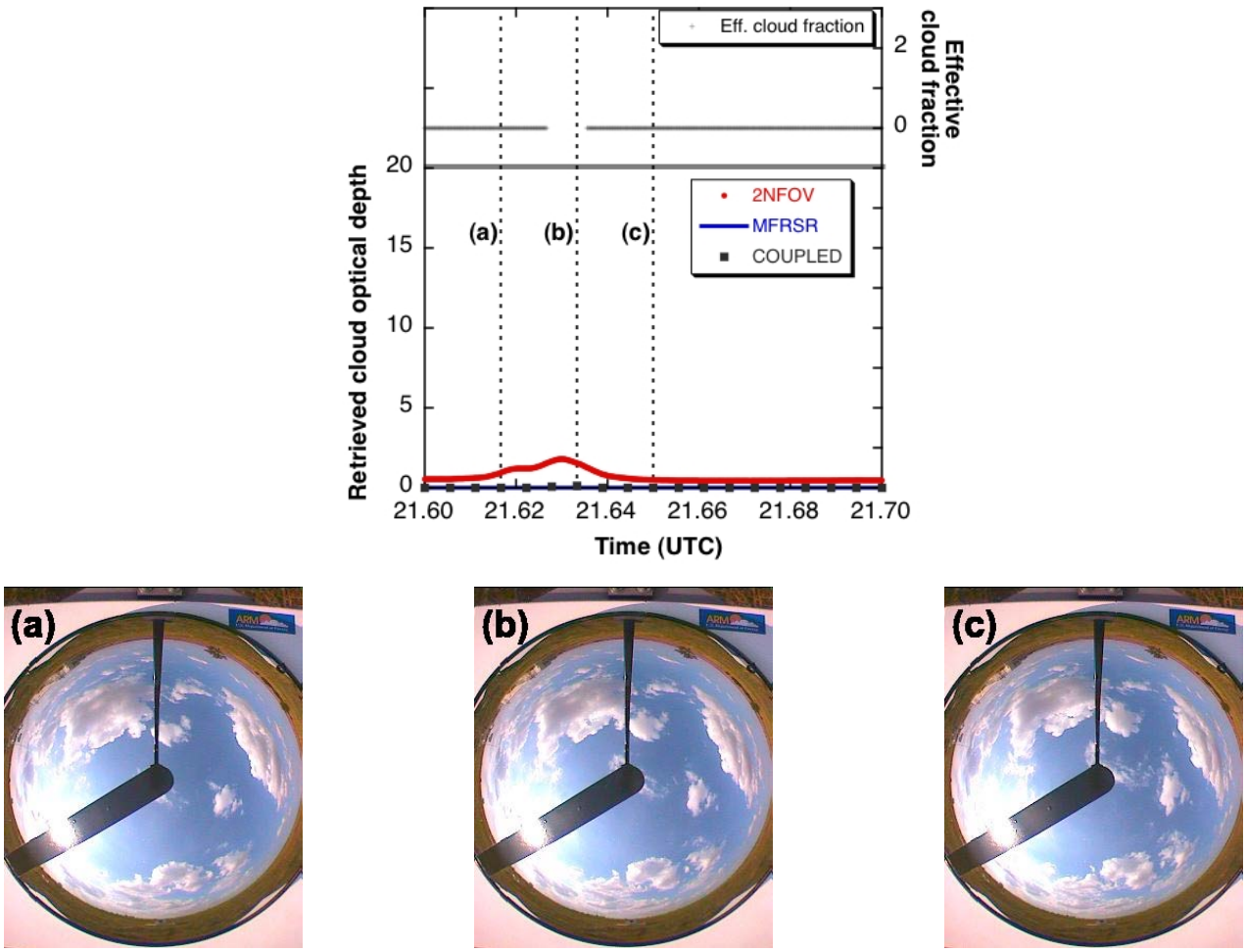

Figure 4. Retrieved cloud optical depths (left y-axis) and effective cloud fractions (right y-axis) at the SGP site for, 21:36:00 - 21:42:00 UTC, September 29, 2004 estimating from the 2NFOV, MFRSR, MWR, and the COUPLED algorithm. Retrieved effective cloud fractions are added at the top panel. Dash lines indicate the time when TSI snapshots were taken: TSI images were taken at (a) 21:37:00, (b) 21:38:00, and (c) 21:39:00 UTC.

Another broken cloud case when clouds moved very rapidly is illustrated for 17:36 to 17:42 UTC of October 28 (Figure 5). These significant cloud transitions are revealed in the retrievals of cloud optical properties from the RED vs. NIR algorithm. However up to now, no comparable observations or retrievals are available to validate our high temporal resolution retrievals. We can only intercompare these retrievals with a coarse resolution.

The microwave radiometer has the most similar field-of-view to the 2NFOV radiometer, and thus we expected substantial similarity in retrievals from these two instruments. When relatively thicker clouds are in the FOV, cloud optical depths inferred from the MWR and 2NFOV are very close (as shown in Figure 5a and b). However, we found that in some cases with thin clouds or no cloud in the FOV (e.g., Figure 5c), the RED vs. NIR algorithm yielded small cloud optical depths, while the MWR suggested relatively large values.

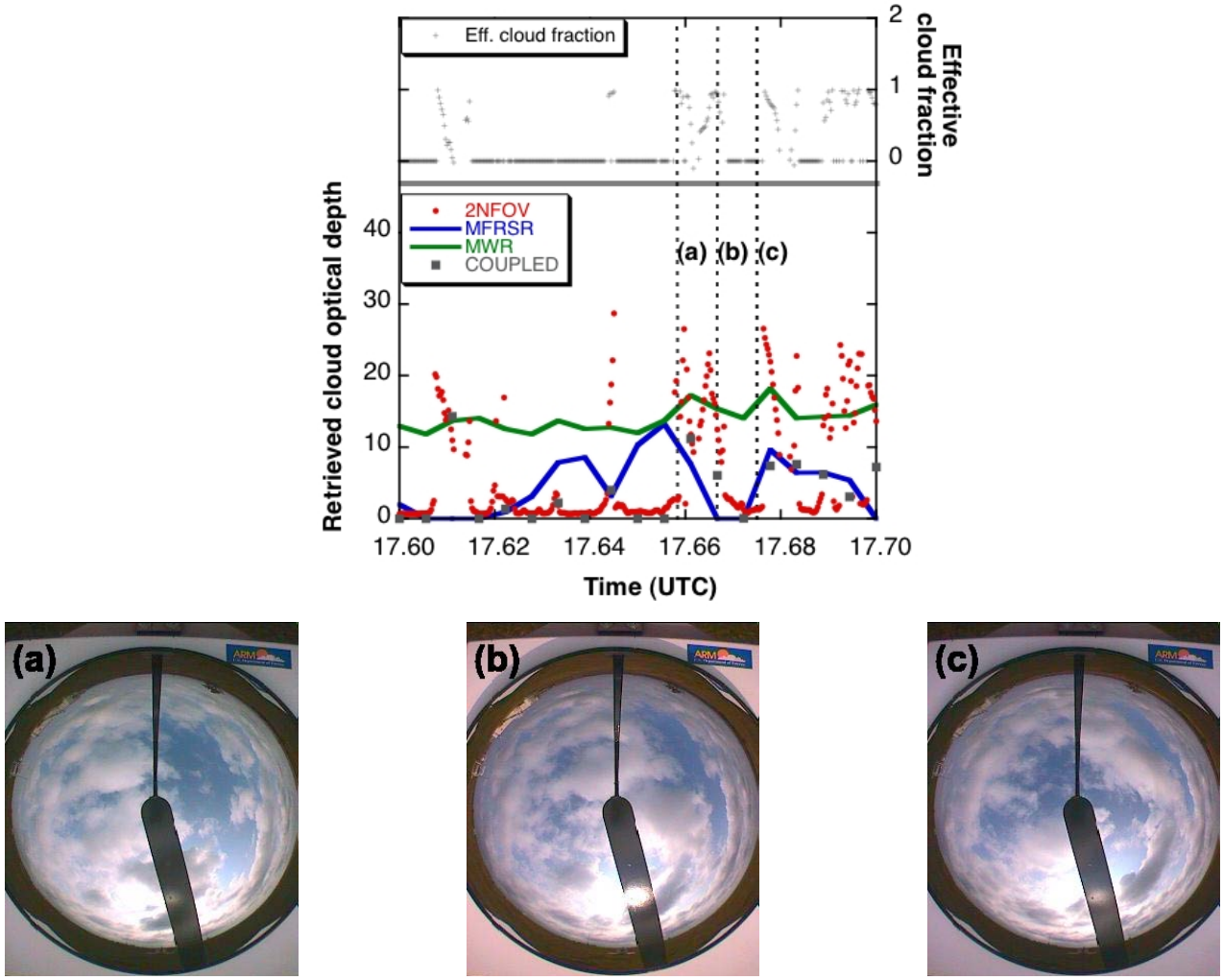

Figure 5. Retrieved cloud optical depths (left y-axis) and effective cloud fractions (right y-axis) at the SGP site for 17:36:00 to 17:42:00, October 28, 2004, estimating from the 2NFOV, MFRSR, MWR, and the COUPLED algorithm. Retrieved effective cloud fractions are added at the top panel. Dash lines indicate the time when TSI snapshots were taken: (a) 17:39:30, (b) 17:40:01, and (c) 17:40:30 UTC.

Retrievals from the COUPLED algorithm demonstrate the influences from both the radiance and flux measurements, as expected. Thus, most retrievals are somewhat closer to values inferred either from the RED vs. NIR algorithm or the MFRSR. Note that a number of retrievals from the RED vs. NIR algorithm suddenly jumped to very large values (above 15) from small cloud optical depths (around 3). We found these situations occurred when cumulus clouds just passed by and the field-of-view was not fully filled by clouds. These problematic situations will be discussed next.

c. Clear-sky contamination

A segment of October 28, 2004 is selected (Figure 6) to illustrate a potential problem arisen from the "narrow" field-of-view, which is not narrow enough in cloud property retrievals. For instance, retrievals show that there are some unreasonably large cloud optical depths around 17.53 UTC. Looking at the center of the TSI image, the left-upper quadrant had some small cumulus clouds at this time frame, but the other three quadrants were clear. This cloud moved outward 30 seconds later as shown in the next TSI snapshot. It is clear that there is no cloud thick enough to produce such large optical depths (up to 40).

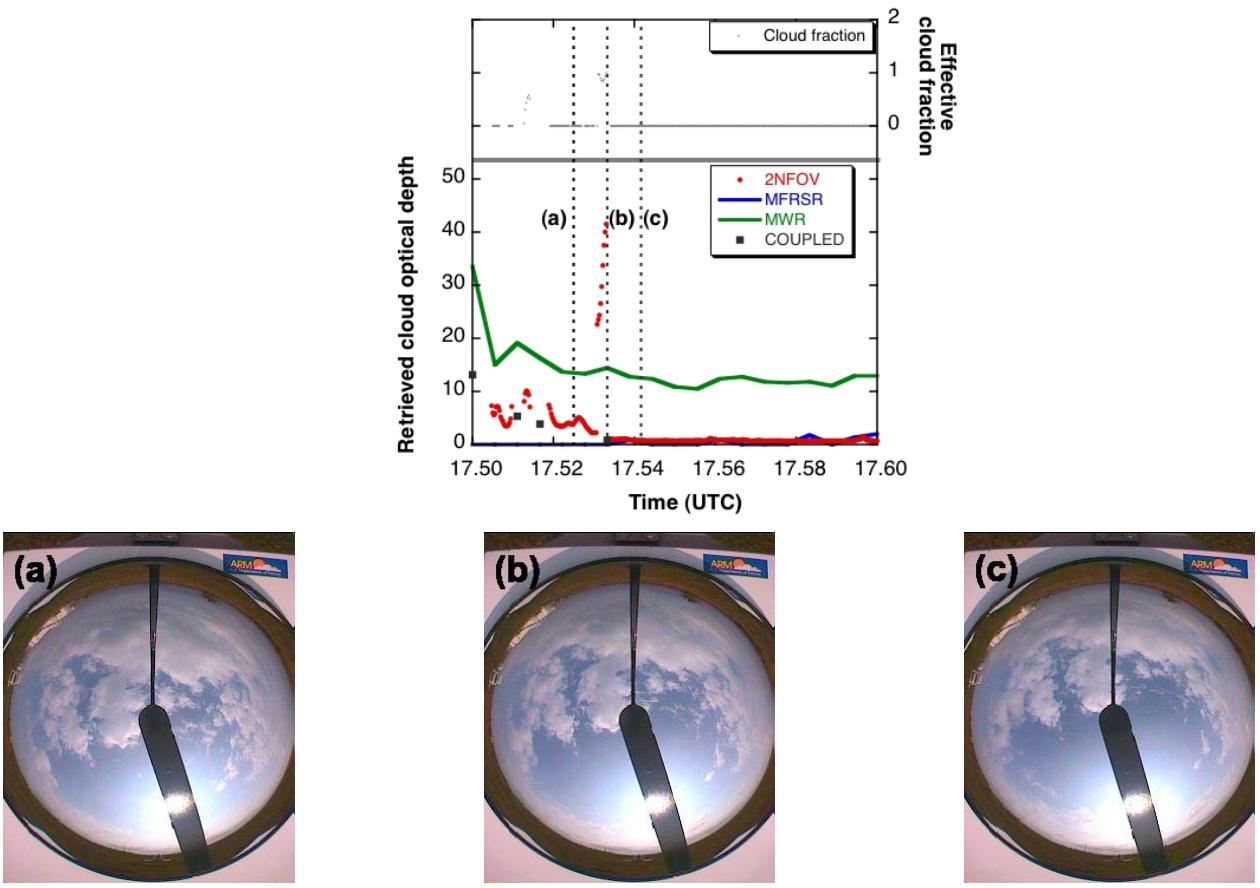

Figure 6. Retrieved cloud optical depths (left y-axis) and effective cloud fractions (right y-axis) at the SGP site for 17:30:00 to 17:42:00,October 28, 2004, estimating from the 2NFOV, MFRSR, MWR, and the COUPLED algorithm. Retrieved effective cloud fractions are added at the top panel. Dash lines indicate the time when TSI snapshots were taken: (a) 17:31:30, (b) 17:32:00, and (c) 17:32:30 UTC.

This retrieval error is attributed to parts of the FOV of the 2NFOV being occupied by the clear sky. The situation with partially cloudy and partially clear within the FOV leads to small radiances at both channels. The RED vs. NIR algorithm fails since it cannot differentiate this situation from optically thick clouds that also produce small radiances. This problem, called the "clear-sky contamination problem" in this paper, has occurred on many other days. Therefore, the FOV of the ARM 2NFOV radiometer has recently been reduced to 1.2° to lower the probabilities of clear-sky contaminations, and will be further tested in the ARM field campaign.

Summary

We have pioneered an algorithm to retrieve cloud optical depth in a fully three-dimensional cloud situation using the new ARM ground-based passive two-channel narrow-field-of-view (NFOV) measurements. Results demonstrate that our algorithm is able to capture local, rapid evolutions of clouds. In addition to cloud optical depth, this algorithm also provides an effective cloud fraction that is crucial for the climate modeling community.

We noticed that when the FOV is not fully filled with clouds, our algorithm retrieves false large cloud optical depths. Therefore, the FOV of the 2NFOV radiometer was just decreased to 1.2° recently. The ARM program will deploy the newest 2NFOV radiometer in a field experiment. This reduced FOV should help to achieve less interferences from clear-sky and cloud edge. Furthermore, the ARM has started building a new six-channel NFOV radiometer, having exactly same wavelengths with the MFRSR. We can expect to extend the principle of the RED vs. NIR algorithm to other surface type, and explore suitable channels to infer cloud optical properties.

Acknowledgments

This research was supported by the Office of Science (BER, U.S. Department of Energy, Interagency Agreement No. DE-AI02-95ER61961.) as part of the Atmospheric Radiation Measurement Program.

Corresponding Author

J. C. Chiu, cchiu@climate.gsfc.nasa.gov, (410) 455-6796

References

Barker, HW, and A Marshak. 2001. "Inferring optical depth of broken clouds above green vegetation using surface solar radiometric measurements." *Journal of Atmospheric Sciences* 58, 2989-3006.

Barker, HW, CF Pavloski, M Ovtchinnikov, and EE Clothiaux. 2004. "Assessing a cloud optical depth retrieval algorithm with model-generated data and the frozen turbulence assumption." *Journal of Atmospheric Science* 61, 2951-2956.

Boers, R. 1997. "Simultaneous retrievals of cloud optical depth and droplet concentration from solar irradiance and microwave liquid." *Journal of Geophysical Research* 102, 29 881–29 891.

Dong, X, TP Ackerman, EE Clothiaux, P Pilewskie, and Y Han. 1997. "Microphysical and radiative properties of boundary layer stratiform clouds deduced from ground-based measurements." *Journal of Geophysical Research* 102, 23829-23843.

Knyazikhin, Y, A Marshak, and RB Myneni. 2005. "3D Radiative transfer in vegetation canopies and cloud-vegetation interaction, in Three-Dimensional Radiative Transfer in Cloudy Atmospheres." edited by A Marshak and AB Davis. pp. 623-658.

Leontieva, E, and K Stamnes. 1994. "Estimations of cloud optical thickness from ground-based measurements of incoming solar radiation in the Arctic." *Journal of Climate* 7, 566–578.

Leontieva, E, and K Stamnes. 1996. "Remote sensing of cloud optical properties from ground-based measurements of transmittance: a feasibility case." *Journal of Applied Meteorology* 35, 2012–2022.

Liou, KN. 2002. "An introduction to atmospheric radiation." Academic Press, 583 pp.

Luo, Y, AP Trishchenko, R Latifovic, and Z Li. 2005. "Surface bidirectional reflectance and albedo properties derived using a land over-based approach with Moderate Resolution Imaging Spectroradiometer observations." *Journal of Geophysical Research* 110, D01106, doi:10.1029/2004JD004741.

Marshak, A and A Davis (Ed.). 2005. "Three-dimensional radiative transfer in cloudy atmospheres." Springer Verlag, 690 pp.

Marshak, A, Y Knyazikhin, KD Evans, and WJ Wiscombe. 2004. "The 'RED versus NIR' plane to retrieve borken-cloud optical depth from ground-based measurements." *Journal of Atmospheric Science* 61, 1911-1925.

Min, QL, and LC Harrison. 1996. "Cloud properties derived from surface MFRSR measurements and comparison with GOES results at the ARM SGP site." *Geophysical Research Letters* 23, 1641–1644.

Petty, GW. 2004. "A First Course in Atmospheric Radiation." In *A First Course in Atmospheric Radiation*. Sundog, Madison, Wisconsin, pp 444.

Ricchiazzi, P, C Gautier, D Lubin. 1995. "Cloud scattering optical depth and local surface albedo in the Antarctic - simultaneous retrieval Using ground-based radiometry." Journal of Geophysical Research 100, 21091-21104.